Article

High-Order Boussinesq Equations for Water Wave Propagation in Porous Media

Ping Wang [1], Zhongbo Liu [2,*], Kezhao Fang [3], Jiawen Sun [1] and Daxun Gou [4]

1   State Environmental Protection Key Laboratory of Marine Ecosystem Restoration, National Marine Environmental Monitoring Center, Dalian 116023, China; wangping@nmemc.org.cn (P.W.); jwsun@nmemc.org.cn (J.S.)
2   College of Transportation Engineering, Dalian Maritime University, Dalian 116026, China
3   State Key Laboratory of Coastal and Offshore Engineering, Dalian University of Technology, Dalian 116024, China; kfang@dlut.edu.cn
4   Liaoning Transportation Affairs Service Center, The Transportation Department of Liaoning Province, Shenyang 110003, China
*   Correspondence: liuzhongbo@dlmu.edu.cn

Abstract: To accurately capture wave dynamics in porous media, the higher-order Boussinesq-type equations for wave propagation in deep water are derived in this paper. Starting with the Laplace equations combined with the linear and nonlinear resistance force of the dynamic conditions on the free surface, the governing equations were formulated using various independent velocity variables, such as the depth-averaged velocity and the velocity at the still water level and at an arbitrary vertical position in the water column. The derived equations were then improved, and theoretical analyses were carried out to investigate the linear performances with respect to phase celerity and damping rate. It is shown that Boussinesq-type models with Padé [4, 4] dispersion can be applied in deep water. A numerical implementation for one-dimensional equations expressed with free surface elevation and depth-averaged velocity is presented. Solitary wave propagation in porous media was simulated, and the computed results were found to be generally in good agreement with the measurements.

Keywords: porous media; wave; Boussinesq equations; dispersion; damping rate

1. Introduction

Human-made porous structures, such as rock breakwaters and revetments, are often built close to the shore to protect coastal buildings and prevent severe coastal erosion. These types of coastal structures partially reflect wave energy and partially dissipate wave energy due to the drag and inertial resistance of the structures, resulting in only partial wave transmission. Therefore, it is important to have a good understanding of how the wave motion interacts with porous structures. Much research has been carried out since 1990, and an excellent review was conducted by Losada et al. [1].

Research on the interaction between waves and porous structures has been successfully carried out using differential approaches such as analytical solutions [2], laboratory measurements [1,3], and numerical modeling [4–7]. Among these works, numerical models based on the Navier–Stokes (RANS) equations and nonlinear shallow water (NLSW) equations are commonly used to calculate wave interaction with porous structures and appear to be more advantageous. RANS models can represent the details of the flow fields of porous structures, as shown in research conducted by Sasikumar et al. [8], but require longer computation times, making the application of RANS models to the interaction between waves and porous structures very challenging at present. In contrast to RANS models, NLSW models are much more computationally efficient as only depth-averaged parameters are calculated, as they can efficiently simulate long waves in a shallow water region but are not suitable for accurately describing short, dispersive waves and are inadequate for

the interactions between waves and porous structures. Mohamed et al. [9] used NLSW models to simulate shallow waves with porosity structures based on the finite volume method. In recent years, smoothed-particle hydrodynamic (SPH) models have also been used to simulate wave propagation; these are meshless and achieve similar accuracy to RANS-type models, and their validity has been demonstrated by Ren et al. [10], but these models still require a huge computational effort, which limits their application in modeling wave propagation in porous structures.

In recent decades, Boussinesq-type models have been significantly enriched and widely applied in modeling the coastal waves and currents in complex bathymetric configurations, such as the FUNWAVE model [11–13] and the MIKE21 BW model [14]. The Boussinesq-type models have better computational efficiency, with their main advantage being the simplification of the three-dimensional problem into the two-dimensional one, as outlined in excellent reviews by Kirby [15], Madsen and Fuhrman [16], Brocchini [17], Kirby [18], and Sun et al. [19]. As stated by Sun et al. [19], the Boussinesq-type models can be classified into two groups: the quasi-three-dimensional (3D) Boussinesq-type models and the two-horizontal-dimension (2HD) models. Sun et al. [19] also summarized the use of Boussinesq-type models for wave propagation over a porous seabed and in multi-layer water with different densities. The use of Boussinesq-type models for wave propagation and evolution on the impermeable seabed [20,21] has been fully developed, and some representative types of these equations include the extended Boussinesq-type models, with improved linear dispersion/shoaling characteristics [22–25]; the second-order nonlinear Boussinesq-type models [26,27]; the so-called fully nonlinear Boussinesq-type models [28–32]; and the extremely dispersive and nonlinear Boussinesq-type models [33–36]. More recently, using the methods proposed in the literature [30,33,35,37], a Boussinesq-type model for interfacial waves over a two-density system has been proposed.

The above Boussinesq-type models with exact linear and nonlinear properties cannot be used directly for wave propagation in porous media. As can be seen, the inclusion of porosity in Boussinesq-type models has rarely been reported. Cruz et al. [38] first proposed a set of weakly nonlinear Boussinesq-type models using depth-averaged velocities in both free and permeable water surfaces to model wave propagation over a permeable seabed. Starting with the Euler equations, Hsiao et al. [39] and Chen [40] independently proposed two sets of higher-order Boussinesq-type equations expressed in terms of velocities at two arbitrary vertical locations. Liu and Sun [41] extended the Boussinesq equations of Hsiao et al. [39] to make them applicable to wave propagation in deeper water. More recently, the composite Boussinesq-type models for use over porous beds were proposed by Klonaris and Memos [42]. However, when the porous structures were sub-aerial with surface-piercing boundaries, the aforementioned Boussinesq-type models could not be applied. For such cases, Hsiao et al. [43] were the first to develop a second-order Boussinesq model for starting to simulate similar conditions, and more recently, Fang et al. [44] developed a Boussinesq-type wave model to simulate the interaction of coastal waves with bottom-mounted porous structures. However, these models (e.g., [43,44]) may not be valid for short-wave propagation from deeper water into shallower water.

To overcome these shortcomings and to fully account for wave dispersion, nonlinearity, and modeling efficiency, it is essential to develop Boussinesq-type models suitable for cases of porous structures that span from deeper water to shallower water. The aim of this study was to develop a Boussinesq-type model that is both valid for wave propagation in deeper water and suitable for wave interactions with a surface-piercing porous structure. By analyzing the above-mentioned Boussinesq-type models and comparing them with the models for waves in impermeable seabed cases, the Boussinesq-type models valid for wave interaction with a surface-penetrating porous structure have the linear and nonlinear resistance forces resulting from the water passing through the porous media. Therefore, we will derive the Boussinesq-type models following the main procedures as developed by Madsen and Schäffer [45].

This paper is organized as follows. The detailed derivation of four sets of Boussinesq-type equations for wave propagation in a porous structure is given in Section 2. In Section 3, the phase celerity and damping rate of the Boussinesq models are theoretically analyzed and compared with the analytical solutions. Numerical implementation of 1D equations and simulation of solitary wave interaction with porous breakwater are carried out to validate the present model in Section 4. Finally, conclusions are drawn in Section 5.

2. Derivation of High Order of Boussinesq-Type Equations

2.1. Governing Equations and Boundary Conditions

The sketch of wave propagation in a porous media is shown in Figure 1, where the computational domain is divided into non-porous media and porous media. In Figure 1, $z = 0$ represents the still water level, $\eta(x, y, t)$ is the free surface elevation (measured at still water level), $h_b(x, y)$ is the depth of the porous media, and $\psi(x, y, z, t)$ denotes the velocity potential in non-porous and porous media.
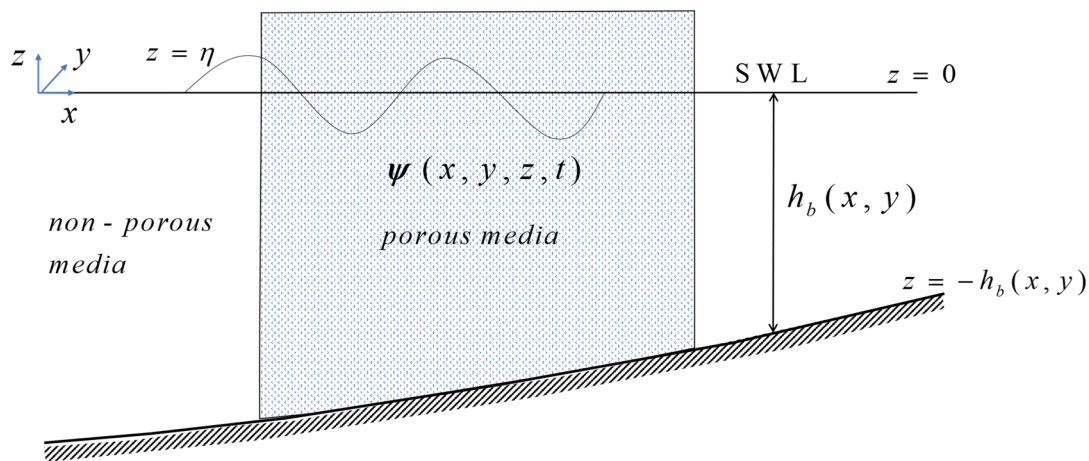

Figure 1. The sketch of wave propagation in porous media.

The flow is assumed to be impressible and irrotational, and the equation of motion inside and outside the porous media is derived by Cruz et al. [38] and can be written as:

$$n\frac{d\boldsymbol{U}_s}{dt} + \frac{1}{\rho}\nabla_3(p_s + \rho gz) + F_r + F_i = 0 \tag{1}$$

where n is the porosity, $n = 1$ represents wave propagation in non-porous media and $n < 1$ represents porous media. $\boldsymbol{U}_s \equiv (u_s, v_s, w_s)$ is the three-dimensional velocity vector, p_s is the pore pressure, ρ is the fluid density, g is the gravity acceleration, $\nabla_3 = (\partial/\partial x, \partial/\partial y, \partial/\partial z)$ is the gradient operator, and $d/d_t = \partial/\partial t + \boldsymbol{U}_s \cdot \nabla_3$ denotes the total derivative. F_r and F_i denote drag resistance and inertial force, respectively, and they are defined as

$$F_r = \alpha_1 \boldsymbol{U}_s + \alpha_2 |\boldsymbol{U}_s| \boldsymbol{U}_s, \quad F_i = (1 - n)(1 + c_m)\frac{d\boldsymbol{U}_s}{dt} \tag{2}$$

where α_1 and α_2 denote coefficients for laminar fluid and turbulence force, respectively, and c_m is the added mass coefficient. Inserting Equation (2) into Equation (1), we can obtain the following equation

$$c_r\frac{d\boldsymbol{U}_s}{dt} + \frac{1}{\rho}\nabla_3(p_s + \rho gz) + \alpha_1 \boldsymbol{U}_s + \alpha_2 |\boldsymbol{U}_s| \boldsymbol{U}_s = 0 \tag{3}$$

where $c_r = n + (1 - n)(1 + c_m/n)$ is the inertial force coefficient.

The mass conservation equation in porous media is

$$\nabla_3 \cdot (n\boldsymbol{U}_s) = 0 \tag{4}$$

If the porosity is assumed to be a constant value, Equation (4) can be written as

$$\nabla_3 \cdot \boldsymbol{U}_s = 0 \tag{5}$$

At the free surface, the dynamic and kinematic conditions are

$$p_s = 0 \qquad z = \eta(x, y, t) \tag{6}$$

$$\frac{d}{dt}(z - \eta) = w_s - \frac{\partial \eta}{\partial t} - \boldsymbol{u}_s \cdot \nabla \eta = 0 \qquad z = \eta(x, y, t) \tag{7}$$

where $\nabla = \left(\frac{\partial}{\partial x}, \frac{\partial}{\partial y}\right)$ is the horizontal gradient operator and $\boldsymbol{u}_s = (u_s, v_s)$ is the corresponding velocity vector at the free surface. At the bottom boundary, we have

$$\boldsymbol{u}_s \cdot \nabla h_b + w_s = 0 \qquad z = -h_b \tag{8}$$

To reduce the number of unknown variables in the derivation, the three-dimensional velocity vector can be replaced by the velocity potential, as shown in the following formula

$$\boldsymbol{U}_s \equiv \nabla_3 \boldsymbol{\psi} \tag{9}$$

The mass conservation equation is thus transformed into the Laplace equations

$$\nabla^2 \boldsymbol{\psi} + \boldsymbol{\psi}_{zz} = 0, \qquad -h_b < z < \eta \tag{10}$$

and Equation (3) can be written as

$$c_r\left(\boldsymbol{\psi}_t + \frac{1}{2}\nabla_3 \boldsymbol{\psi}^2\right) + p_s + gz + \alpha \boldsymbol{\psi} = 0 \tag{11}$$

According to Equation (11), the dynamic and kinematic conditions at the free surface can be written as follows

$$c_r\left(\boldsymbol{\psi}_t + \frac{1}{2}\nabla_3 \boldsymbol{\psi}^2\right) + g\eta + \alpha \boldsymbol{\psi} = 0 \quad z = \eta(x, y, t) \tag{12}$$

$$\boldsymbol{\psi}_z = \frac{\partial \eta}{\partial t} - \nabla \boldsymbol{\psi} \cdot \nabla \eta = 0 \qquad z = \eta(x, y, t) \tag{13}$$

And at the bottom, the boundary condition is

$$\nabla \boldsymbol{\psi} \cdot \nabla h_b + \boldsymbol{\psi}_z = 0 \qquad z = -h_b \tag{14}$$

Thus, Equations (10) and (12)–(14) are the motion equations and boundary conditions inside the porous media expressed by velocity potential.

2.2. Dimensionless Equations

To obtain the dimensionless equations, we normalize the variables using characteristic wave amplitude a, characteristic water depth h_0, and characteristic wavelength l_0 as follows

$$x' = \frac{x}{l_0}, y' = \frac{y}{l_0}, z' = \frac{z}{h_0}, h_b' = \frac{h_b}{h_0}, \eta' = \frac{\eta}{a}, \ t' = \frac{t\sqrt{gh_0}}{l_0}, \boldsymbol{\psi}' = \frac{\boldsymbol{\psi}}{a\sqrt{gh_0}} \frac{l_0}{h_0} \tag{15}$$

Two parameters representing nonlinearity and dispersion are introduced in the derivation as

$$\varepsilon = \frac{a}{h_0}, \quad \mu = \frac{h_0}{l_0} \tag{16}$$

Omitting primes for simplicity, the Equations (10) and (12)–(14) can be written as

$$\mu^2 \nabla^2 \boldsymbol{\psi} + \boldsymbol{\psi}_{zz} = 0, \qquad -h_b < z < \varepsilon\eta \tag{17}$$

$$\mu^2 (c_r \boldsymbol{\psi}_t + \alpha\boldsymbol{\psi} + \eta) + \varepsilon c_r \frac{1}{2}[\mu^2 (\nabla \boldsymbol{\psi})^2 + \boldsymbol{\psi}_z{}^2] = 0 \qquad z = \varepsilon\eta \tag{18}$$

$$\mu^2 (\eta_t + \varepsilon\nabla\boldsymbol{\psi} \cdot \nabla\eta) = \boldsymbol{\psi}_z \qquad z = \varepsilon\eta \tag{19}$$

$$\mu^2 \nabla\boldsymbol{\psi} \cdot \nabla h_b + \boldsymbol{\psi}_z = 0, \qquad z = -h_b \tag{20}$$

Notice that by setting $c_r = 1$ and $\alpha = 0$, Equation (18) recovers to the expressions presented in the original paper of Madsen and Schäffer [45].

2.3. Power Series Solution to the Laplace Equations

The main advantage of the Boussinesq equations is to simplify the three-dimensional problem into a two-dimensional one. We first expand the velocity potential as

$$\boldsymbol{\psi}(x,y,z,t) = \sum_{n=0} z^n \psi^{(n)}(x,y,t) \tag{21}$$

The first and second order of the potential derivatives can be expressed as

$$\nabla\boldsymbol{\psi}(x,y,z,t) = \sum_{n=0} z^n \nabla\psi^{(n)}(x,y,t) \tag{22}$$

$$\nabla^2\boldsymbol{\psi}(x,y,z,t) = \sum_{n=0} z^n \nabla^2\psi^{(n)}(x,y,t) \tag{23}$$

$$\boldsymbol{\psi}_z(x,y,z,t) = \sum_{n=0} (n+1)z^n \psi^{(n+1)}(x,y,t) \tag{24}$$

$$\boldsymbol{\psi}_{zz}(x,y,z,t) = \sum_{n=0} (n+2)(n+1)z^n \psi^{(n+2)}(x,y,t) \tag{25}$$

Inserting Equations (23) and (24) into Equation (17), we obtain a recurrence relation as

$$\psi^{(n+2)} = -\frac{1}{(n+1)(n+2)}\mu^2\nabla^2\psi^{(n)} \quad n = 0,1,2,\ldots\ldots \tag{26}$$

The velocity potential is thus expressed as follows

$$\boldsymbol{\psi}(x,y,z,t) = \sum_{n=0} (-1)^n \mu^{2n}\left(\frac{z^{2n}}{(2n)!}\nabla^{2n}\psi^{(0)} + \frac{z^{2n+1}}{(2n+1)!}\nabla^{2n}\psi^{(1)}\right) \tag{27}$$

Equation (27) indicates that the velocity potential can be expressed by the expansion $\psi^{(0)}$ and $\psi^{(1)}$. The derivatives of velocity potential over horizontal plane (x,y) and vertical plane z direction can be written as

$$\boldsymbol{u}_s(x,y,z,t) = \sum_{n=0} (-1)^n \mu^{2n}\left(\frac{z^{2n}}{(2n)!}\nabla(\nabla^{2n-2}(\nabla\cdot\boldsymbol{u}_s)) + \frac{z^{2n+1}}{(2n+1)!}\mu^2\nabla(\nabla^{2n}w_s)\right) \tag{28}$$

$$w_s(x,y,z,t) = \sum_{n=0} (-1)^n \mu^{2n+2}\left(-\frac{z^{2n+1}}{(2n+1)!}\nabla^{2n}(\nabla\cdot\boldsymbol{u}_s) + \frac{z^{2n}}{(2n)!}\nabla^{2n}w_s\right) \tag{29}$$

where $\boldsymbol{u}_s \equiv \nabla \psi^{(0)}, \quad w_s \equiv (1/\mu^2)\psi^{(1)}$, i.e.,

$$\boldsymbol{u}_s(x,y,0,t) = \boldsymbol{u}_s, \quad w_s(x,y,0,t) = \mu^2 w_s \tag{30}$$

Inserting Expression (29) into Equation (20), we obtain

$$w_s + \sum_{n=0} (-1)^n \mu^{2n} \nabla \cdot \left(\frac{h_b^{2n+1}}{(2n+1)!} \nabla(\nabla^{2n-2}(\nabla \cdot \boldsymbol{u}_s))) - \mu^2 \frac{h_b^{2n+2}}{(2n+2)!} \nabla(\nabla^{2n} w_s) \right) = 0 \tag{31}$$

Similarly, $w_s(x,y,t) = \sum\limits_{m=0} \mu^{2n} w_s{}^{(n)}(x,y,t)$ is introduced and truncated to the order of $O(\mu^6)$, and we have

$$
\begin{aligned}
w_s(x,y,t) = \quad & -\nabla \cdot (h_b \boldsymbol{u}_s) + \mu^2 \nabla \cdot \left\{ \tfrac{1}{6} h_b{}^3 \nabla(\nabla \cdot \boldsymbol{u}_s) - \tfrac{1}{2} h_b{}^2 \nabla[\nabla \cdot (h_b \boldsymbol{u}_s)] \right\} \\
& + \mu^4 \nabla \cdot \left\{ \tfrac{1}{24} h_b{}^4 \nabla[\nabla^2(\nabla \cdot (h_b \boldsymbol{u}_s))] - \tfrac{1}{120} h_b{}^5 \nabla[\nabla^2(\nabla \cdot \boldsymbol{u}_s)] \right. \\
& \left. + \tfrac{1}{2} h_b{}^2 \nabla[\nabla \cdot (\tfrac{1}{6} h_b{}^3 \nabla(\nabla \cdot \boldsymbol{u}_s) - \tfrac{1}{2} h_b{}^2 \nabla(\nabla \cdot (h_b \boldsymbol{u}_s)))] \right\} + O(\mu^6)
\end{aligned}
\tag{32}
$$

2.4. Boussinesq Equations in Terms of Velocity at the Free Surface $\hat{\boldsymbol{u}}_s$

Inserting Equations (27) and (28) into Equation (18), applying the horizontal gradient operator, and eliminating $w_s(x,y,t)$ using Expression (32) under the assumption that $\varepsilon = O(\mu)$, we have

$$\hat{\boldsymbol{u}}_{st} + \alpha/c_r \hat{\boldsymbol{u}}_s + \nabla\eta/c_r + \varepsilon \frac{1}{2} \nabla(\hat{\boldsymbol{u}}_s)^2 + \mu^2 \left\{ \varepsilon T_{21} + \varepsilon^2 T_{22} + \varepsilon^3 T_{23} \right\} + \mu^4(\varepsilon T_{41}) = O(\mu^6, \varepsilon^2 \mu^4) \tag{33}$$

$$T_{21} = \nabla[-\eta \nabla \cdot (h_b \hat{\boldsymbol{u}}_{st}) - \alpha/c_r \eta \, \nabla \cdot (h_b \hat{\boldsymbol{u}}_s) + \frac{1}{2}(\nabla \cdot (h_b \hat{\boldsymbol{u}}_s))^2] \tag{34a}$$

$$T_{22} = \nabla[-\frac{1}{2}\eta^2 \nabla \cdot \hat{\boldsymbol{u}}_{st} - \frac{1}{2}\alpha/c_r \eta^2 \nabla \cdot \hat{\boldsymbol{u}}_s - \eta \hat{\boldsymbol{u}}_s \cdot \nabla\nabla \cdot (h_b \hat{\boldsymbol{u}}_s) + \eta \nabla \cdot (h_b \hat{\boldsymbol{u}}_s) \nabla \cdot \hat{\boldsymbol{u}}_s] \tag{34b}$$

$$T_{23} = \nabla[-\frac{1}{2}\eta^2 \hat{\boldsymbol{u}}_s \cdot \nabla\nabla \cdot \hat{\boldsymbol{u}}_s + \frac{1}{2}(\eta \nabla \cdot \hat{\boldsymbol{u}}_s)^2] \tag{34c}$$

$$T_{41} = \nabla[\eta \nabla \cdot (h_b{}^2 \Gamma_t) + \alpha/c_r \eta \nabla \cdot (h_b{}^2 \Gamma) - \nabla \cdot (h_b{}^2 \Gamma) \nabla \cdot (h_b \boldsymbol{u}_s)] \tag{34d}$$

$$\Gamma = \frac{1}{6} h_b \nabla(\nabla \cdot \boldsymbol{u}_s) - \frac{1}{2}\nabla(\nabla \cdot (h_b \boldsymbol{u}_s)) \tag{34e}$$

Similarly, using the same simplification method, we can obtain the depth-integrated continuity equations

$$\eta_t + \nabla \cdot Q = 0 \tag{35}$$

where

$$
\begin{aligned}
Q \quad \equiv \quad & \int_{-h_b}^{\varepsilon\eta} \nabla \boldsymbol{\psi} \, dz \\
= \quad & \hat{\boldsymbol{u}}_s(h_b + \varepsilon\eta) - \mu^2 \left\{ \tfrac{1}{6}(\varepsilon^3 \eta^3 + h_b{}^3) \nabla(\nabla \cdot \hat{\boldsymbol{u}}_s) + \tfrac{1}{2}(\varepsilon^2 \eta^2 - h_b{}^2) \nabla[\nabla \cdot (h_b \hat{\boldsymbol{u}}_s)] \right\} \\
& + \mu^4 \left\{ \tfrac{1}{2}(\varepsilon^2 \eta^2 - h_b{}^2) \nabla[\nabla \cdot (h_b{}^2 \Gamma)] + \tfrac{1}{24}(\varepsilon^4 \eta^4 - h_b{}^4) \nabla[\nabla^2(\nabla \cdot (h_b \hat{\boldsymbol{u}}_s))] \right. \\
& \left. + \tfrac{1}{120}(\varepsilon^5 \eta^5 + h_b{}^5) \nabla[\nabla^2(\nabla \cdot \hat{\boldsymbol{u}}_s)] \right\} + O(\mu^6)
\end{aligned}
\tag{36}
$$

2.5. Boussinesq Equations in Terms of Depth-Averaged Velocity $\overline{\boldsymbol{u}}_s$

The depth-averaged velocity $\overline{\boldsymbol{u}}_s$ is defined as

$$\overline{\boldsymbol{u}}_s = \frac{1}{h_b + \varepsilon\eta} \int_{-h_b}^{\varepsilon\eta} \nabla\boldsymbol{\psi}\,dz \tag{37}$$

and it can be expressed in terms of $\hat{\boldsymbol{u}}_s$ as

$$\begin{aligned}
\overline{\boldsymbol{u}}_s &= \hat{\boldsymbol{u}}_s + \mu^2\left\{\tfrac{1}{2}(h_b - \varepsilon\eta)\nabla[\nabla\cdot(h_b\hat{\boldsymbol{u}}_s)] - \tfrac{1}{6}(h_b{}^2 - \varepsilon h_b\eta + \varepsilon^2\eta^2)\nabla(\nabla\cdot\hat{\boldsymbol{u}}_s)\right\} \\
&\quad + \mu^4\left\{-\tfrac{1}{2}(h_b - \varepsilon\eta)\nabla[\nabla\cdot(h_b{}^2\Gamma)] - \tfrac{1}{24}(h_b{}^3 - \varepsilon h_b{}^2\eta + \varepsilon^2\eta^2 h_b - \varepsilon^3\eta^3)\nabla[\nabla^2(\nabla\cdot(h_b\hat{\boldsymbol{u}}_s))]\right. \\
&\quad \left. + \tfrac{1}{120}(h_b{}^4 - \varepsilon h_b{}^3\eta + \varepsilon^2\eta^2 h_b{}^2 - \varepsilon^3\eta^3 h_b + \varepsilon^4\eta^4)\nabla[\nabla^2(\nabla\cdot\hat{\boldsymbol{u}}_s)]\right\} + O(\mu^6)
\end{aligned} \tag{38}$$

From the expression, we can obtain

$$\begin{aligned}
\hat{\boldsymbol{u}}_s &= \overline{\boldsymbol{u}}_s - \mu^2\left\{\tfrac{1}{2}(h_b - \varepsilon\eta)\nabla[\nabla\cdot(h_b\overline{\boldsymbol{u}}_s)] - \tfrac{1}{6}(h_b{}^2 - \varepsilon h_b\eta + \varepsilon^2\eta^2)\nabla(\nabla\cdot\overline{\boldsymbol{u}}_s)\right\} \\
&\quad + \mu^4\left\{\ \tfrac{1}{24}(h_b{}^3 - \varepsilon h_b{}^2\eta + \varepsilon^2\eta^2 h_b - \varepsilon^3\eta^3)\nabla[\nabla^2(\nabla\cdot(h_b\overline{\boldsymbol{u}}_s))]\right. \\
&\quad - \tfrac{1}{120}(h_b{}^4 - \varepsilon h_b{}^3\eta + \varepsilon^2\eta^2 h_b{}^2 - \varepsilon^3\eta^3 h_b + \varepsilon^4\eta^4)\nabla[\nabla^2(\nabla\cdot\overline{\boldsymbol{u}}_s)] \\
&\quad - \tfrac{1}{2}(h_b - \varepsilon\eta)\nabla[\nabla\cdot(\tfrac{1}{2}\varepsilon\eta h_b\nabla(\nabla\cdot(h_b\overline{\boldsymbol{u}}_s)) - \tfrac{1}{6}(\varepsilon\eta h_b{}^2 - \varepsilon^2\eta^2 h_b)\nabla(\nabla\cdot\overline{\boldsymbol{u}}_s))] \\
&\quad - \tfrac{1}{6}(h_b{}^2 - \varepsilon h_b\eta + \varepsilon^2\eta^2)\nabla[\nabla\cdot(\tfrac{1}{2}(h_b - \varepsilon\eta)\nabla(\nabla\cdot(h_b\overline{\boldsymbol{u}}_s)) \\
&\quad \left. - \tfrac{1}{6}(h_b{}^2 - \varepsilon h_b\eta + \varepsilon^2\eta^2)\nabla(\nabla\cdot\overline{\boldsymbol{u}}_s))]\right\} + O(\mu^6)
\end{aligned} \tag{39}$$

The continuity equation in terms of $\overline{\boldsymbol{u}}_s$ is

$$\eta_t + \nabla\cdot[(h_b + \varepsilon\eta)\overline{\boldsymbol{u}}_s] = 0 \tag{40}$$

Inserting Expression (39) into Equations (33) and (34), and introducing the mild-slope assumption $|\nabla^n(h_b)| = O(\mu)$, $n = 1, 2, 3$, we obtain

$$\begin{aligned}
\overline{\boldsymbol{u}}_{st} + \alpha/c_r\overline{\boldsymbol{u}}_s + \nabla\eta/c_r + \varepsilon\tfrac{1}{2}\nabla(\overline{\boldsymbol{u}}_s)^2 + \mu^2\{T_{M20} + \varepsilon T_{M21} + \varepsilon^2 T_{M22} + \varepsilon^3 T_{M23}\} \\
+ \mu^4(T_{M40} + \varepsilon T_{M41}) = O(\mu^6, \varepsilon^2\mu^4)
\end{aligned} \tag{41}$$

$$T_{M20} = h_b\Gamma_t + \alpha/c_r h_b\Gamma \tag{42a}$$

$$T_{M21} = -\eta\Gamma_t - \alpha/c_r\eta\Gamma + \nabla[\overline{\boldsymbol{u}}_s\cdot(h_b\Gamma) - \eta\nabla\cdot(h_b\overline{\boldsymbol{u}}_{st}) - \alpha/c_r\eta\,\nabla\cdot(h_b\overline{\boldsymbol{u}}_s) + \tfrac{1}{2}(\nabla\cdot(h_b\overline{\boldsymbol{u}}_s))^2] \tag{42b}$$

$$\begin{aligned}
T_{M22} &= \tfrac{1}{6}\eta^2\nabla(\nabla\cdot\overline{\boldsymbol{u}}_{st}) + \alpha/c_r\eta^2\nabla(\nabla\cdot\overline{\boldsymbol{u}}_s) - \tfrac{1}{3}\eta\nabla\cdot(h_b\overline{\boldsymbol{u}}_s)\nabla(\nabla\cdot\overline{\boldsymbol{u}}_s) + \nabla\cdot(\eta\overline{\boldsymbol{u}}_s)\Gamma \\
&\quad + \nabla[\eta\overline{\boldsymbol{u}}_s\cdot\Gamma - \tfrac{1}{2}\eta^2\nabla\cdot\overline{\boldsymbol{u}}_{st} - \tfrac{1}{2}\alpha/c_r\eta^2\nabla\cdot\overline{\boldsymbol{u}}_s - \eta\overline{\boldsymbol{u}}_s\cdot\nabla\nabla\cdot(h_b\overline{\boldsymbol{u}}_s) + \eta\nabla\cdot(h_b\overline{\boldsymbol{u}}_s)\,\nabla\cdot\overline{\boldsymbol{u}}_s]
\end{aligned} \tag{42c}$$

$$T_{M23} = -\tfrac{1}{3}\eta\nabla\cdot(\eta\overline{\boldsymbol{u}}_s)\nabla(\nabla\cdot\overline{\boldsymbol{u}}_s) + \nabla[-\tfrac{1}{3}\eta^2\overline{\boldsymbol{u}}_s\cdot\nabla\nabla\cdot\overline{\boldsymbol{u}}_s + \tfrac{1}{2}(\eta\nabla\cdot\overline{\boldsymbol{u}}_s)^2] \tag{42d}$$

$$\begin{aligned}
T_{M40} &= \tfrac{1}{24}h_b{}^3\nabla(\nabla^2(\nabla\cdot(h_b\overline{\boldsymbol{u}}_{st}))) - \tfrac{1}{120}h_b{}^4\nabla(\nabla^2(\nabla\cdot\overline{\boldsymbol{u}}_{st})) + \tfrac{1}{6}h_b{}^2\nabla(\nabla\cdot(h_b\Gamma_t)) \\
&\quad + \alpha/c_r[\tfrac{1}{24}h_b{}^3\nabla(\nabla^2(\nabla\cdot(h_b\overline{\boldsymbol{u}}_s))) - \tfrac{1}{120}h_b{}^4\nabla(\nabla^2(\nabla\cdot\overline{\boldsymbol{u}}_s)) + \tfrac{1}{6}h_b{}^2\nabla(\nabla\cdot(h_b\Gamma))]
\end{aligned} \tag{42e}$$

$$\begin{aligned}
T_{M41} &= \tfrac{1}{45}h_b{}^3\eta\nabla(\nabla^2(\nabla\cdot\overline{\boldsymbol{u}}_{st})) - \tfrac{1}{9}h_b{}^3\nabla(\nabla\cdot(\eta\nabla(\nabla\cdot\overline{\boldsymbol{u}}_{st}))) \\
&\quad + \alpha/c_r[\tfrac{1}{45}h_b{}^3\eta\nabla(\nabla^2(\nabla\cdot\overline{\boldsymbol{u}}_s)) - \tfrac{1}{9}h_b{}^3\nabla(\nabla\cdot(\eta\nabla(\nabla\cdot\overline{\boldsymbol{u}}_s)))] \\
&\quad - \tfrac{1}{45}h_b{}^4\nabla\cdot\overline{\boldsymbol{u}}_s\nabla(\nabla^2(\nabla\cdot\overline{\boldsymbol{u}}_s)) + \tfrac{1}{9}h_b{}^4\nabla[\nabla\cdot(\nabla\cdot\overline{\boldsymbol{u}}_s(\nabla(\nabla\cdot\overline{\boldsymbol{u}}_s)))] \\
&\quad + \tfrac{1}{18}h_b{}^4\nabla(\nabla(\nabla\overline{\boldsymbol{u}}_s))^2
\end{aligned} \tag{42f}$$

$$\Gamma = \tfrac{1}{6}h_b\nabla(\nabla\cdot\overline{\boldsymbol{u}}_s) - \tfrac{1}{2}\nabla(\nabla\cdot(h_b\overline{\boldsymbol{u}}_s)) \tag{42g}$$

2.6. Boussinesq Equations in Terms of Velocity at an Arbitrary Water Column $\boldsymbol{u}_{sa}$

Keeping the order accurate up to $O(\mu^4)$, the velocity at an arbitrary water depth can be written as

$$\boldsymbol{\psi}(x, y, z_\alpha h_b, t) = \psi^{(0)} - \mu^2 z \nabla \cdot (h_b \nabla \psi^{(0)}) \quad - \frac{1}{2}\mu^2 z^2 h_b{}^2 \nabla^2 \psi^{(0)} + O(\mu^4) \tag{43}$$

The expression of $\boldsymbol{u}_{s\alpha}$ in terms of $\hat{\boldsymbol{u}}_s$ is given

$$\boldsymbol{u}_{s\alpha} = \hat{\boldsymbol{u}}_s - \mu^2 \left\{ z_\alpha \, h_b \nabla \nabla \cdot (h_b \hat{\boldsymbol{u}}_s) \quad + \frac{1}{2} z_\alpha{}^2 h_b{}^2 \nabla \nabla \cdot \hat{\boldsymbol{u}}_s \right\} \tag{44}$$

So, we can obtain the following expression

$$\hat{\boldsymbol{u}}_s = \boldsymbol{u}_{s\alpha} + \mu^2 \left\{ z_\alpha \, h_b \nabla \nabla \cdot (h_b \boldsymbol{u}_{s\alpha}) \quad + \frac{1}{2} z_\alpha{}^2 h_b{}^2 \nabla \nabla \cdot \boldsymbol{u}_{s\alpha} \right\} \tag{45}$$

Inserting (45) into momentum Equation (33), we have

$$\boldsymbol{u}_{sat} + \alpha/c_r \boldsymbol{u}_{sa} + \nabla \eta / c_r + \varepsilon \frac{1}{2} \nabla (\boldsymbol{u}_{sa})^2 + \mu^2 \left(T_{s20} + \varepsilon T_{s21} + \varepsilon^2 T_{s22} + \varepsilon^3 T_{s23} \right) = O(\mu^4) \tag{46}$$

$$T_{s20} = \Gamma_{sat} + \alpha/c_r \Gamma_{sa} \tag{47a}$$

$$T_{s21} = \nabla[-\eta \nabla \cdot (h_b \boldsymbol{u}_{s\alpha t}) - \alpha/c_r \, \eta \, \nabla \cdot (h_b \boldsymbol{u}_{s\alpha}) + \frac{1}{2} (\nabla \cdot (h_b \boldsymbol{u}_{s\alpha}))^2 + \boldsymbol{u}_{s\alpha} \cdot \Gamma_{s\alpha}] \tag{47b}$$

$$T_{s22} = \nabla[-\frac{1}{2}\eta^2 \nabla \cdot \boldsymbol{u}_{s\alpha t} - \frac{1}{2}\alpha/c_r \eta^2 \nabla \cdot \boldsymbol{u}_{s\alpha} - \eta \boldsymbol{u}_{s\alpha} \cdot \nabla \nabla \cdot (h_b \boldsymbol{u}_{s\alpha}) + \eta \nabla \cdot (h_b \boldsymbol{u}_{s\alpha}) \nabla \cdot \boldsymbol{u}_{s\alpha}] \tag{47c}$$

$$T_{s23} = \nabla[-\frac{1}{2}\eta^2 \boldsymbol{u}_{s\alpha} \cdot \nabla \nabla \cdot \boldsymbol{u}_{s\alpha} + \frac{1}{2}(\eta \nabla \cdot \boldsymbol{u}_{s\alpha})^2] \tag{47d}$$

$$\Gamma_{s\alpha} = z_\alpha \, h_b \nabla \nabla \cdot (h_b \boldsymbol{u}_{s\alpha}) \quad + \frac{1}{2} z_\alpha{}^2 h_b{}^2 \nabla \nabla \cdot \boldsymbol{u}_{s\alpha} \tag{47e}$$

Inserting (45) into continuity Equation (35), we obtain

$$\eta_t + \nabla \cdot [(h_b + \varepsilon \eta) \boldsymbol{u}_{sa} + \mu^2 [(\frac{1}{2}h_b{}^2 + z_\alpha h_b{}^2 + \varepsilon z_\alpha \eta h_b - \frac{1}{2}\varepsilon^2 \eta^2) \nabla (\nabla \cdot (h_b \boldsymbol{u}_{sa}))$$
$$(\frac{1}{2} z_\alpha{}^2 h_b{}^3 - \frac{1}{6}h_b{}^3 + \varepsilon z_\alpha{}^2 \eta h_b{}^2 - \frac{1}{6}\varepsilon^3 \eta^3) \nabla (\nabla \cdot \boldsymbol{u}_{sa})] = 0 \tag{48}$$

2.7. Boussinesq Models Extended to Deeper Water Depth

In order to extend the applicability of the models to deeper water, the technique presented by Madsen and Schäffer [45] is used to improve the derived model. This method has been widely used in the literature to obtain the improved Boussinesq-type equations for open water problems [45,46].

2.7.1. The Improvement of Equations in Terms of Depth-Averaged Velocity

(1) Keeping at order $O(\mu^2)$

Keeping at order $O(\mu^2)$, the depth-averaged velocity Equations (40)–(42) have identical dispersion as the classical Boussinesq equations [47] and are only valid in the shallow water region. To extend its application range, we introduce the following Expression [48].

$$T_{exta1} = \beta_2 (h_b + \varepsilon \eta) \mu^2 \nabla \nabla \cdot ((h_b + \varepsilon \eta)(\bar{\boldsymbol{u}}_{st} + \nabla \eta / c_r + \alpha/c_r \bar{\boldsymbol{u}}_s + \varepsilon \nabla (\bar{\boldsymbol{u}}_s{}^2)/2))$$
$$+ \beta_1 (h_b + \varepsilon \eta)^2 \mu^2 \nabla \nabla \cdot (\bar{\boldsymbol{u}}_{st} + \nabla \eta / c_r + \alpha/c_r \bar{\boldsymbol{u}}_s + \varepsilon \nabla (\bar{\boldsymbol{u}}_s{}^2)/2) = O(\mu^4) \tag{49}$$

where β_1 and β_2 are dispersive parameters.

By adding Equation (49) to Equation (41), the resulting equation is written as

$$\overline{\boldsymbol{u}}_{st} + \alpha/c_r \overline{\boldsymbol{u}}_s + \nabla\eta/c_r + \varepsilon\frac{1}{2}\nabla(\overline{\boldsymbol{u}}_s)^2 + \mu^2\left\{T_{M20} + \varepsilon T_{M21} + \varepsilon^2 T_{M22} + \varepsilon^3 T_{M23}\right\} + T_{extra1} = O(\mu^4) \tag{50}$$

(2)　Keeping at order $O(\mu^4)$

Following Madsen and Schäffer [45], we add the following terms into Equation (41)

$$
\begin{aligned}
T_{exta2} = \ & (\gamma_2 - \gamma_1)h_b{}^2\mu^2[\nabla\nabla\cdot(\overline{\boldsymbol{u}}_{st} + \nabla\eta/c_r + \alpha/c_r\overline{\boldsymbol{u}}_s + \varepsilon\nabla(\overline{\boldsymbol{u}}_s{}^2)/2) + \mu^2\nabla\nabla\cdot(T_{M20}) \\
& +\varepsilon\mu^2\nabla\nabla\cdot(T_{M21})]\gamma_2 h_b\mu^2\big\{\nabla\nabla\cdot[h_b(\overline{\boldsymbol{u}}_{st} + \nabla\eta/c_r + \alpha/c_r\overline{\boldsymbol{u}}_s + \varepsilon\nabla(\overline{\boldsymbol{u}}_s{}^2)/2)] \\
& +\mu^2\nabla\nabla\cdot(h_b T_{M20}) + \varepsilon\mu^2\nabla\nabla\cdot(h_b T_{M21})\big\} + \gamma_3 h_b{}^4\mu^4\big\{\nabla[\nabla^2(\nabla\cdot(\overline{\boldsymbol{u}}_{st} + \nabla\eta/c_r + \alpha/c_r\overline{\boldsymbol{u}}_s \\
& +\varepsilon\nabla(\overline{\boldsymbol{u}}_s{}^2)/2))]\big\} + \gamma_4 h_b{}^3\nabla h_b\mu^4[\nabla^2(\nabla\cdot(\overline{\boldsymbol{u}}_{st} + \nabla\eta/c_r + \alpha/c_r\overline{\boldsymbol{u}}_s))] = O(\mu^6, \varepsilon^2\mu^4)
\end{aligned}
\tag{51}
$$

where γ_1 and γ_3 are dispersive parameters, γ_2 and γ_4 are shoaling parameters. The enhanced version of Equation (41) can be written as

$$
\begin{aligned}
\overline{\boldsymbol{u}}_{st} + \alpha/c_r\overline{\boldsymbol{u}}_s + \nabla\eta/c_r + \varepsilon\tfrac{1}{2}\nabla(\overline{\boldsymbol{u}}_s)^2 + \mu^2\left\{T_{M20} + \varepsilon T_{M21} + \varepsilon^2 T_{M22} + \varepsilon^3 T_{M23}\right\} \\
+\mu^4(T_{M40} + \varepsilon T_{M41}) + T_{extra2} = O(\mu^6, \varepsilon^2\mu^4)
\end{aligned}
\tag{52}
$$

2.7.2. The Improvement of Equations in Terms of $\boldsymbol{u}_{s\alpha}$

Neglecting high-order terms, Equations (46)–(48) are written as follows

$$\eta_t + \nabla\cdot[(h + \varepsilon\eta)\boldsymbol{u}_{s\alpha}] = O(\mu^2) \tag{53}$$

$$\boldsymbol{u}_{s\alpha t} + \varepsilon\boldsymbol{u}_{s\alpha}\cdot\nabla\boldsymbol{u}_{s\alpha} + \nabla\eta + \alpha/c_r\boldsymbol{u}_{s\alpha} = O(\mu^2) \tag{54}$$

Also following Madsen and Schäffer [45], we have

$$
\begin{aligned}
T_{extra3} = \ & (\delta_2 - \delta_1)\mu^2\nabla\cdot\big\{h_b{}^2\nabla[\eta_t + \nabla\cdot((h_b + \varepsilon\eta)\boldsymbol{u}_{sa})]\big\} \\
& -\delta_2\mu^2\big\{h_b{}^2[\eta_t + \nabla\cdot((h_b + \varepsilon\eta)\boldsymbol{u}_{sa})\big\} = O(\mu^4)
\end{aligned}
\tag{55}
$$

$$
\begin{aligned}
T_{extra4} = \ & (\delta_4 - \delta_3)\mu^2(h_b + \varepsilon\eta)^2\nabla^2[\boldsymbol{u}_{s\alpha t} + \varepsilon\boldsymbol{u}_{s\alpha}\cdot\nabla\boldsymbol{u}_{s\alpha} + \nabla\eta/c_r + \alpha/c_r\boldsymbol{u}_{s\alpha}] \\
& -\delta_4\mu^2(h_b + \varepsilon\eta)\nabla^2\big\{(h_b + \varepsilon\eta)[\boldsymbol{u}_{s\alpha t} + \varepsilon\boldsymbol{u}_{s\alpha}\cdot\nabla\boldsymbol{u}_{s\alpha} + \nabla\eta/c_r + \alpha/c_r\boldsymbol{u}_{s\alpha}\big\} = O(\mu^4)
\end{aligned}
\tag{56}
$$

Adding Expression (55) to Equation (46) and Expression (56) to Equation (48), we obtain

$$\boldsymbol{u}_{s\alpha t} + \alpha/c_r\boldsymbol{u}_{s\alpha} + \nabla\eta/c_r + \varepsilon\frac{1}{2}\nabla(\boldsymbol{u}_{s\alpha})^2 + \mu^2\left\{T_{s0} + \varepsilon T_{s1} + \varepsilon^2 T_{s2} + \varepsilon^3 T_{s3}\right\} + T_{extra4} = O(\mu^4) \tag{57}$$

$$
\begin{aligned}
\eta_t + \nabla\cdot[(h_b + \varepsilon\eta)\boldsymbol{u}_{sa} + \mu^2[(\tfrac{1}{2}h_b{}^2 + z_\alpha h_b{}^2 + \varepsilon z_\alpha\eta h_b - \tfrac{1}{2}\varepsilon^2\eta^2)\nabla(\nabla\cdot(h_b\boldsymbol{u}_{sa})) \\
(\tfrac{1}{2}z_\alpha{}^2 h_b{}^3 - \tfrac{1}{6}h_b{}^3 + \varepsilon z_\alpha{}^2\eta h_b{}^2 - \tfrac{1}{6}\varepsilon^3\eta^3)\nabla(\nabla\cdot\boldsymbol{u}_{sa})] + T_{extra3} = O(\mu^4)
\end{aligned}
\tag{58}
$$

In summary, four sets of higher-order Boussinesq models for wave propagation in a porous structure have been derived, i.e., Model 1, Equations (40) and (50); Model 2, Equations (40) and (52); Model 3, Equations (46) and (48); and Model 4, Equations (57) and (58). By neglecting the drag and inertial force induced by the porosity, the four models presented here recover those of Madsen and Schäffer [45]. Compared with the Boussinesq-type models in the literature, Models 2 and 4 are the new Boussinesq-type models that are not presented in any literature. Model 3 can be seen as a slightly different version of Hsiao et al. [43], while Model 1 can be seen as an alternative choice to the Boussiensq-type model of Hsiao et al. [43]. Meanwhile, Models 1 and 3 have more accuracy in regards to second-order nonlinear terms compared with Fang et al. [44].

3. Dispersive Analysis on a Horizontal Bottom

The dispersive analysis of the four sets of Boussinesq models is performed on a horizontal bed in one dimension, neglecting the nonlinear terms and focusing on the phase velocity and damping rate. Following a similar procedure in Hsiao et al. [43], we can obtain the following dispersion expressions for the different models.

For Model 1, the dispersive expression is

$$\omega^2(c_r + \alpha_1 i/\omega) = gKh_b \frac{1 + (\beta_1 + \beta_2)K^2 h_b^2}{1 + (1/3 + \beta_1 + \beta_2)K^2 h_b^2} \tag{59}$$

where ω denotes wave frequency and $K = k_r + ik_i$ is the complex wave number ($i^2 = -1$).

For Model 2, the dispersive expression is

$$\omega^2(c_r + \alpha_1 i/\omega) = gKh_b \frac{1 + \gamma_1 K^2 h_b^2 + \gamma_3 K^4 h_b^4}{1 + (1/3 + \gamma_1)K^2 h_b^2 + (\gamma_3 + \gamma_1/3 - 1/45)K^4 h_b^4} \tag{60}$$

For Model 3, we have the following expression

$$\omega^2(c_r + \alpha_1 i/\omega) = gKh_b \frac{1 - (1/3 + B)K^2 h_b^2}{1 - BK^2 h_b^2} \tag{61}$$

where $B = z_\alpha + z_\alpha^2/2$.

For Model 4, the dispersive expression is

$$\omega^2(c_r + \alpha_1 i/\omega) = gKh_b \frac{1 + (\delta_1 + \delta_3 - B - 1/3)K^2 h_b^2 + \delta_1(\delta_3 - B - 1/3)K^4 h_b^4}{1 + (\delta_1 + \delta_3 - B)K^2 h_b^2 + \delta_3(\delta_1 - B)K^4 h_b^4} \tag{62}$$

If we choose $B = -(1/3 + \beta_1 + \beta_2)$, the dispersion expressions of Model 1 and Model 3 are equivalent. Similarly, the expression of Model 2 is equivalent to that of Model 4 if the parameters are chosen appropriately. Therefore, in the following section, we will focus on Model 1 and Model 2. As suggested by Madsen and Schäffer [45], these dispersion expressions can be closer to the Padé [2, 2] or Padé [4, 4] expansion of the Stokes analytic solutions without considering the porosity effect, if appropriate parameter values are chosen. The coefficients are summarized in Table 1, where two sets of parameter values are given for Model 1.

Table 1. The determined values for coefficient in different models.

Model Sets	Parameter Values
1	$\beta_1 = -0.0013$, $\beta_2 = -0.0654$ (I) or $\beta_1 = 0.0073$, $\beta_2 = -0.064$ (II)
2	$\gamma_1 = 1/9$, $\gamma_2 = 0.146488$, $\gamma_3 = 1/945$, $\gamma_4 = 0.00798359$
3	$B = -0.4$ or $B = -0.395$
4	$\delta_1 = 0.101$, $\delta_3 = 0.039$, $B = -0.305$, $\delta_3 = 0.082$ *, $\delta_4 = 0.162$ *

Note: * The two parameters are determined by reanalysis of the shoaling property, which differs from Madsen and Schäffer [45].

The following analytic dispersive Expression [43] is adopted to evaluate the accuracy of the models

$$\omega^2(c_r + \alpha_1 i/\omega) = gK\tanh(Kh_b) \tag{63}$$

Phase celerity ($c = \omega/k_r$) of the different models is compared to the analytic solution for $\alpha_1 = 0.2$, 2, and 4 s^{-1} in Figures 2–4 (where c is normalized by the analytic value), where Model 1 uses the two set group parameters in Table 1. It can be seen from the figures that Model 2 presents much more accurate results than Model 1, and the maximum error is only 2.5% when the applicable range of water depth is $k_r h = 6.0$ The applicable range of water depth for Model 1 using the second set of parameter value is $k_r h \leq 4.05$, 4.57, 1.58 with a

5% tolerance error for three considered cases, which is higher than that using the first set of parameter value $k_r h \leq 3.2$, 3.75, 1.67.
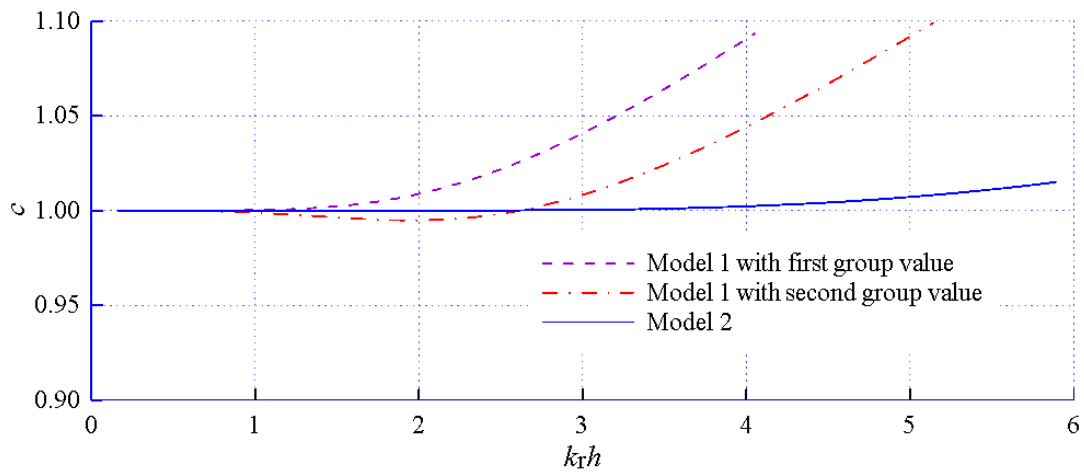
Figure 2. Non-dimensional wave celerity versus water depth ($\alpha_1 = 0.2, \ c_r = 1$).
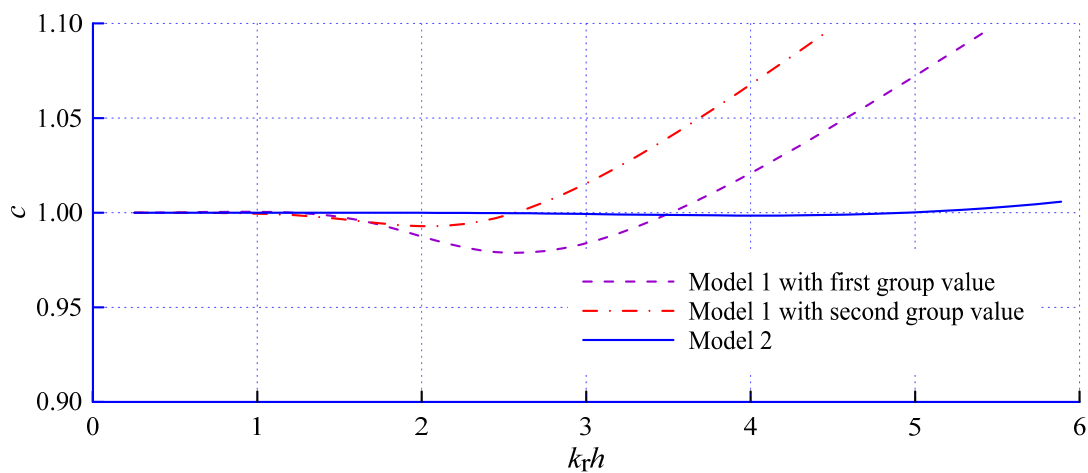
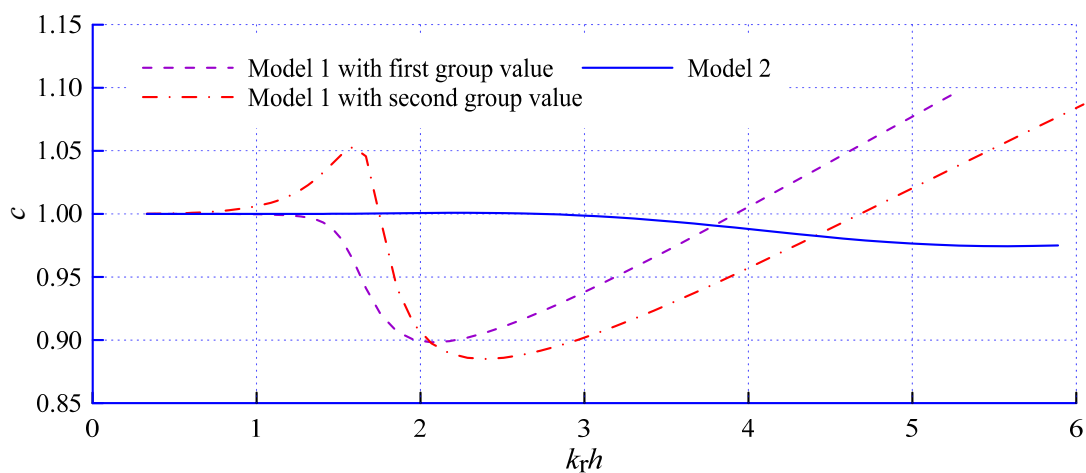**Figure 3.** Non-dimensional wave celerity versus water depth ($\alpha_1 = 2, \ c_r = 1$).

Figure 4. Non-dimensional wave celerity versus water depth ($\alpha_1 = 4, \ c_r = 1$).

Defining $c(k_i)$ as the ratio of imaginary wave number between the model equations and analytic solutions, we could obtain the variation trend of $c(k_i)$ with water depth for

Models 1 and 2, as shown in Figures 5–7 for α_1 = 0.2, 2, and 4 s^{-1}. Model 2 again presents better results than Model 1. The figures show that Model 2 is applicable for water depth $k_r h \leq 4.19, \ 4.41, \ 4.98$ for three cases within 2% error, whilst Model 1 with the first set of parameter values is only applicable for $k_r h \leq 2.0, \ 2.16, \ 1.55$ with 5% error, and with the second set of values only for $k_r h \leq 2.62, \ 2.68, \ 1.52$. According to the above analysis, Model 2 is better adapted to deep water conditions, and its accuracy in deep water varies for different linear force coefficients.
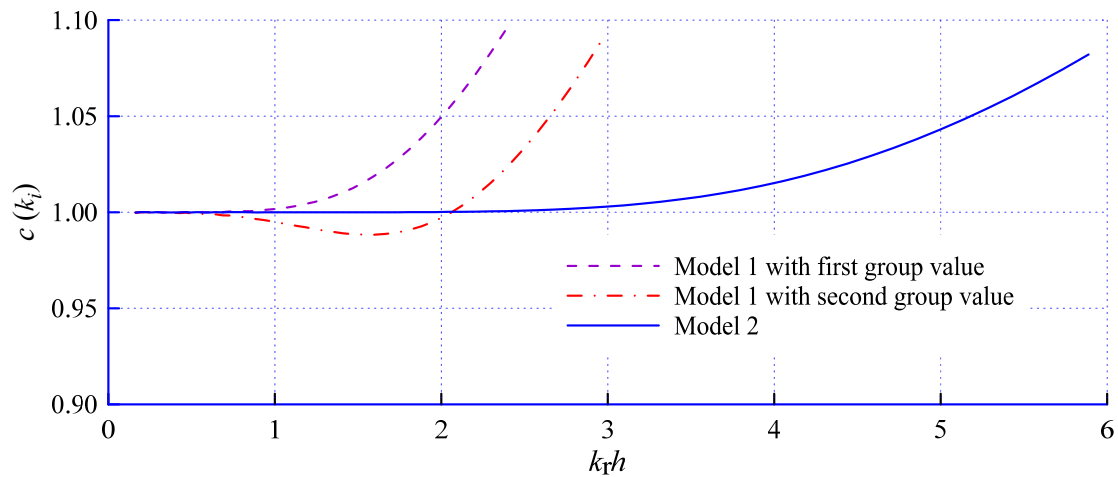
Figure 5. Non-dimensional imaginary wave number versus water depth ($\alpha_1 = 0.2, \ c_r = 1$).
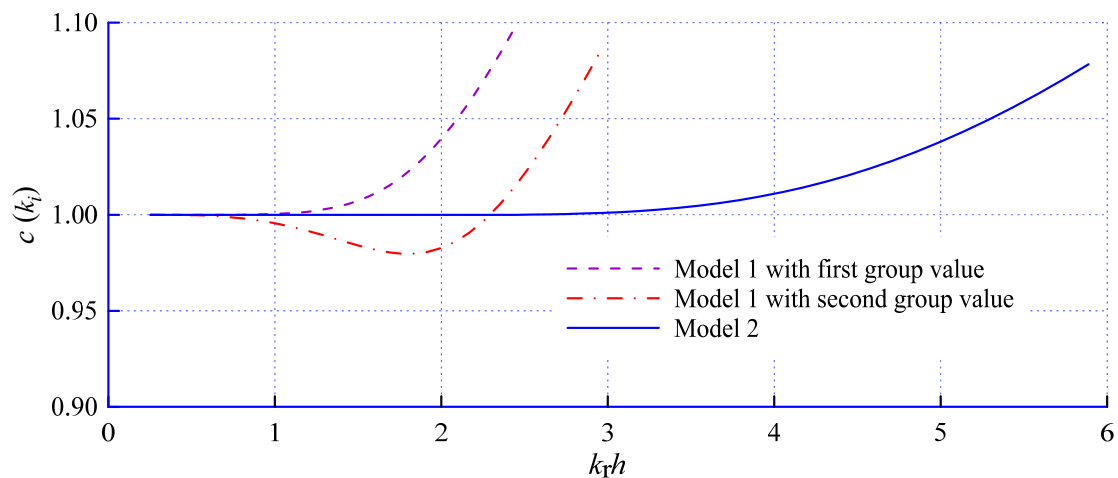
Figure 6. Non-dimensional imaginary wave number versus water depth ($\alpha_1 = 2, \ c_r = 1$).

The above comparisons are carried out without considering the effect of the inertial force coefficient c_r, now let us discuss its effect. From the expression $c_r = 1 + (1 - n)c_m$, we can know that $c_r = 1$ is the minimum value. For $\alpha_1 = 1$, the phase celerity of Model 2 is compared against the analytical solutions for c_r = 1, 1.1, 1.2, and 1.3, which is plotted in Figure 8. It shows that the applicable water depth decreases with the increase in c_r, and the value of the inertial force coefficient c_r greatly affects the results with the increase in the water depth.
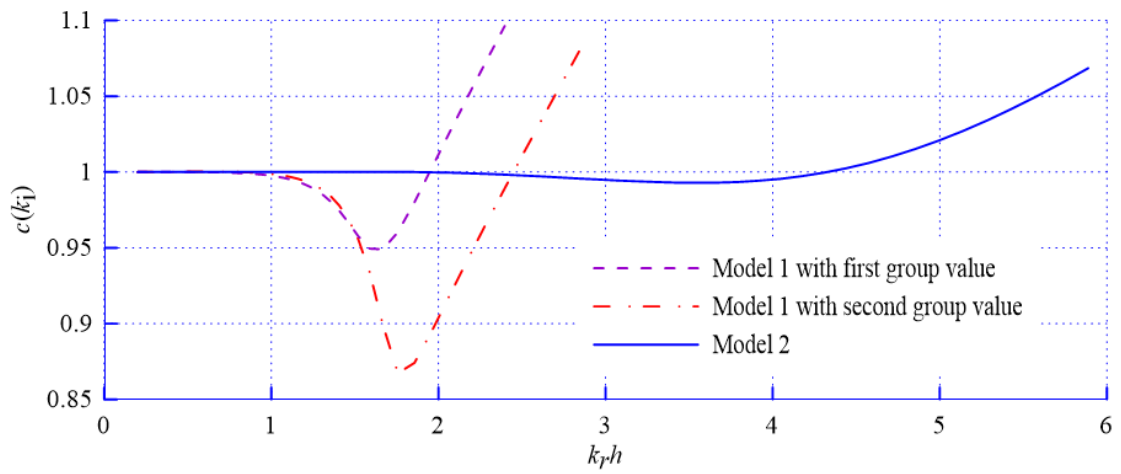
Figure 7. Non-dimensional imaginary wave number versus water depth ($\alpha_1 = 4$, $c_r = 1$).
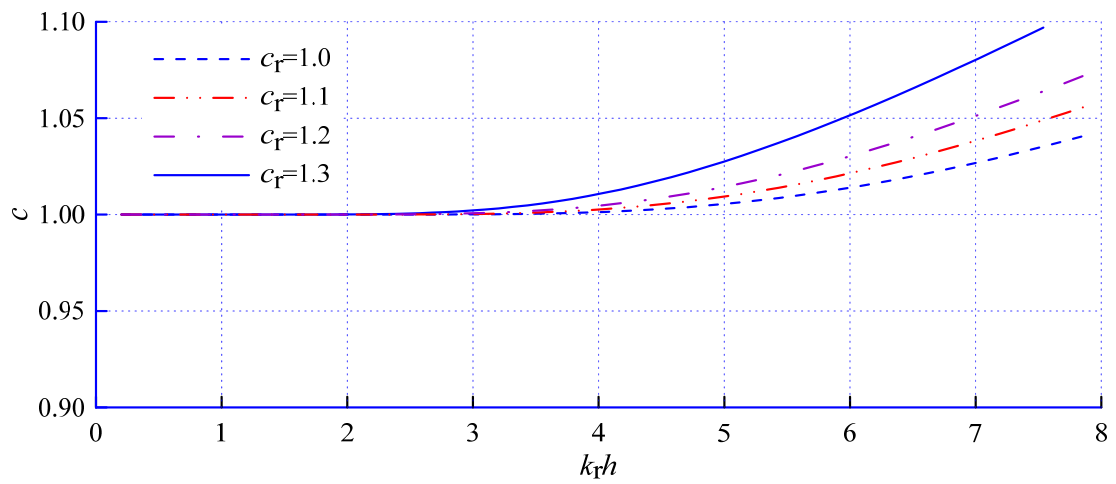
(**a**) Phase celerity.
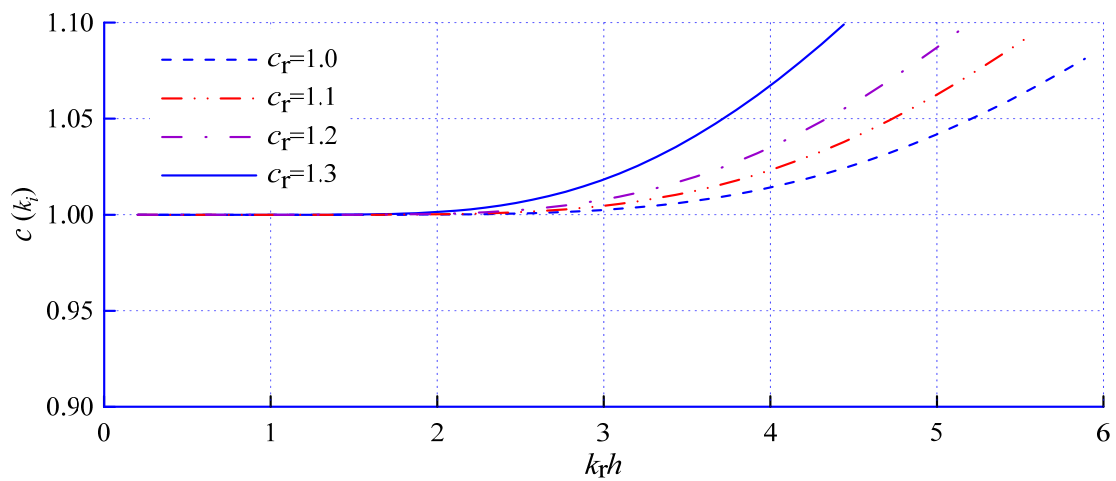
(**b**) Imaginary wave number (damping rate).

Figure 8. The effect of c_r on wave phase celerity and imaginary wave number.

4. Numerical Implementation and Validation

4.1. Numerical Implementation

Considering the overall accuracy of the derived model equations, the one-dimensional version of Model 2 is chosen for numerical implementation. The details of the numerical implementation are given in Kirby et al. [49], with a summary of the core procedures provided for clarity.

The one-dimensional equations of Model 2 are discretized on uniform grids. Higher-order finite difference formulations are used to approximate both the temporal and spatial derivatives. A composite fourth-order Adams–Bashforth–Moulton integration scheme is used for time marching. In the calculation of η and $\boldsymbol{u}$ values at time step $n + 1$, the third-order Adams–Bashforth time scheme is used for the prediction step, and the fourth-order Adams–Moulton scheme is used for the correction step, which is:

$$\eta^{n+1} - \eta^n = \frac{\Delta t}{12}\left(23 f^n - 16 f^{n-1} + 5 f^{n-2}\right) \tag{64}$$

$$\eta^{n+1} - \eta^n = \frac{\Delta t}{24}\left(9 f^{n+1} + 19 f^n - 5 f^{n-1} + f^{n-2}\right) \tag{65}$$

where the superscript n denotes the time step corresponding to the parameter value at time $n \times \Delta t$ and $n + 1$ corresponds to the parameter value at time $(n + 1) \times \Delta t$, f represents the remaining terms in Equations (40) and (52) except the time derivative term.

The derivatives of the space in Equations (40) and (52) are discretized by the 4th order Taylor formats as Equations (66) and (67), which uses 5-point data on the spatial grid, so the velocity components are solved by a bandwidth of 5 broadband solution.

$$f_x = \left(-f_{i+2} + 8 f_{i+1} - 8 f_{i-1} + f_{i+2}\right)/(12 \Delta x) + O(\Delta x)^4 \tag{66}$$

$$f_{xx} = \left(-f_{i-2} + 16 f_{i+1} - 30 f_i + 16 f_{i-1} - f_{i+2}\right)/(12 \Delta x)^2 + O(\Delta x)^4 \tag{67}$$

To enhance numerical stability, the model is solved using a predictor–corrector iterative approach. During the correction stage, the process is repeated until the difference in calculated variables between the two iterations reaches a pre-determined value, typically 0.0001. And the convergence of the iterations is accelerated by using an over-relaxation technique proposed by Kirby et al. [49].

Sponger layers are placed on either side of the numerical flume to absorb wave energy and wave generation occurs internally in the computational domain through the addition of a source function to the mass continuity equation. In this paper, we numerically simulate the propagation of a solitary wave in a porous media, due to the transient characteristics of the solitary wave, the surface elevation and velocities of the solitary wave are directly specified in the computational domain as the initial conditions to generate solitary waves, which is:

$$\eta(t) = H \sec h^2\left(\sqrt{\frac{3H}{4h^3}}(x - ct)\right) \tag{68}$$

$$c = \sqrt{gH}\left(1 + \frac{1}{2}\frac{H}{h}\right) \approx \sqrt{g(H + h)} \tag{69}$$

$$u = \sqrt{gh}\frac{\eta}{h} \tag{70}$$

where η is the water surface change; H is the solitary wave height; h is the water depth; t is the time; c is the wave speed; g is the acceleration of gravity. u is the solitary wave of any mass in the water body of the horizontal velocity.

4.2. Model Validation

The experimental data of the solitary wave interaction with the porous breakwater were obtained by Vidal et al. [50], which has been used to verify the numerical models of Lynett et al. [4] and Lin and Karunarathna [51]. The sketch of the solitary wave interaction with the porous breakwater is shown in Figure 9, where H and h are the wave height and still water depth respectively, and a, d_{50}, and n are the porous structure width, mean diameter, and material porosity. Due to the transient nature of solitary waves, incident and reflected waves do not superimpose in the flume. Wave heights of reflected and transmitted waves on the left and right sides of the porous structure can be directly obtained. Therefore, the calculated reflection coefficient is defined as $K_r = H_L/H_0$, and the transmission coefficient is defined as $K_t = H_R/H_0$, where H_0 is the input wave height of the solitary wave in the wave generation region, and H_L is the wave height on the left side of the solitary wave after passing through the porous structure, H_R is the wave height on the right side of the solitary wave. The numerical results were also compared with the experimental data.
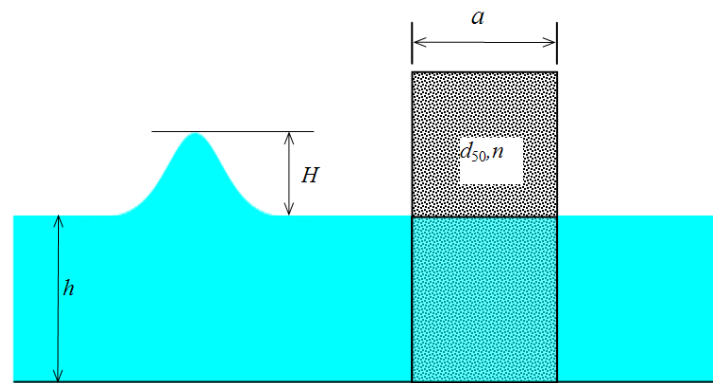
Figure 9. The sketch of solitary wave interaction with a porous breakwater in the experiments by Vidal et al. [50] and Lynett et al. [4].

In the experiment of Vidal et al. [50], the porous breakwater width is 20 cm or 40 cm, and the water depth ranges from 25 cm to 32 cm. The material porosity is 0.44 with two particle diameters $d_{50} = 1.43$ cm and 2.43 cm. In the numerical simulation, the space interval is 0.01 m, and the time interval is 0.005 s. By setting $\alpha_1 = 18$ s^{-1} and $\alpha_2 = 234.45$ m for the $d_{50} = 1.43$ cm case, and $\alpha_1 = 6.23$ s^{-1} and $\alpha_2 = 137.97$ m for the $d_{50} = 2.43$ cm case, the reflection coefficient and transmission coefficient are calculated numerically using Model 2, as shown in Figure 10. For the breakwater with $d_{50} = 2.43$ cm, both the calculated reflection and transmission coefficients are in good agreement with the experimental results. However, for the breakwater with $d_{50} = 1.43$ cm, the calculated reflection coefficients are slightly larger than the experimental data, and the calculated transmission coefficients are slightly smaller than the experimental data, but the trend with wave height (H/h) is consistent with the measured values. Considering the errors introduced by the modeling assumptions and parameters, the model developed in this paper can better simulate the wave interaction with porous structures which has surface-piercing boundaries.

The experiments of Lynett et al. [4] are nearly identical to those of Vidal et al. [50], where four types of porous breakwaters were tested. The gravels in two of the tests had mean diameters of 1.6 and 2.0 cm, and the breakwater length was 15 cm. The mean diameters of the others were 1.6 and 2.0 cm, with a breakwater length of 30 cm. The porosity of the porous media was $n = 0.5$. The water depth was 10 cm. The solitary waves had amplitudes between 1–4 cm. The reflection and transmission coefficient are computed using the free surface time series recorded at 1 m in front of and 1 m behind the breakwater. In the numerical simulation, the spatial interval is 0.01 m, and the time interval is 0.005 s. For $d_{50} = 1.6$ cm, $\alpha_1 = 9.5$ s^{-1} and $\alpha_2 = 200$ m are used, and for $d_{50} = 2.0$ cm, $\alpha_1 = 8$ s^{-1} and $\alpha_2 = 160$ m are used. Figure 11 shows the numerical reflection and transmission coefficients

and the measurements from Lynett et al. [4]. For the 15 cm breakwater, both the calculated reflection and transmission coefficients are in good agreement with the experimental results. However, for the 30 cm breakwater, only the reflection coefficients are in good agreement with the experimental data. The numerical results for the thin breakwater are slightly better than those for the wide breakwater. In general, the agreements between the model results and the experiment data are acceptable after choosing the appropriate coefficients.
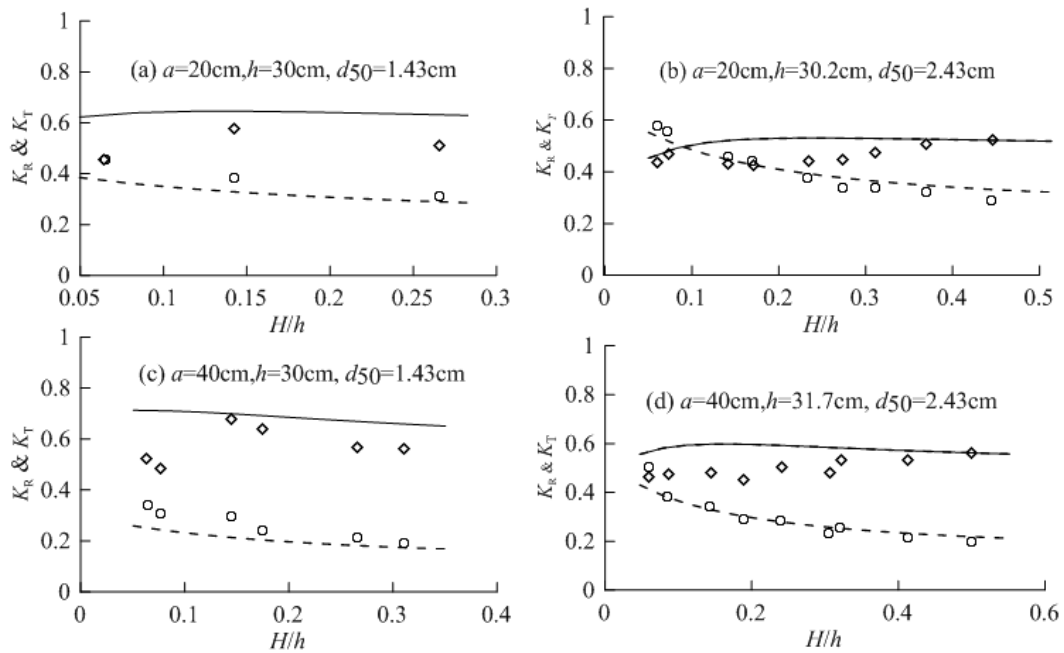
Figure 10. The comparison between computed (line) and measured (points) reflection coefficient (solid line and rhombus) and transmission coefficient (dashed line and circle) in Vidal et al.'s experiment [50].
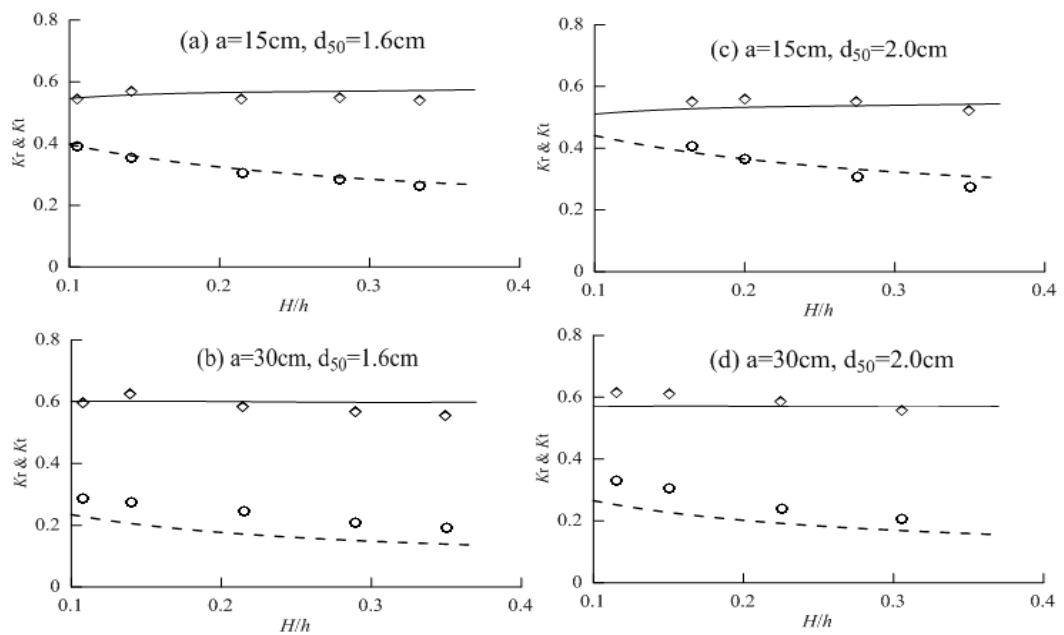
Figure 11. The comparison between computed (line) and measured (points) reflection coefficient (solid line and rhombus) and transmission coefficient (dashed line and circle) in Lynett et al.'s experiment [4].

5. Conclusions

To accurately capture the wave motion in porous structures, four sets of Boussinesq-type equations with different linear and nonlinear performances are derived by including the drag resistance and inertial force induced by the media porosity. Two of them can be considered slightly different versions of Hsiao et al. [43], and the others are the new Boussinesq-type models, which have more accuracy of the second-order nonlinear terms compared to Fang et al. [44]. Two Boussinesq-type models (Mode 2 and Model 4) have Padé [4, 4] dispersion with accurate second or fourth-order nonlinearity, while the other Boussinesq-type models (Mode 1 and Model 3) have Padé [2, 2] dispersion with accurate second-order nonlinearity.

The phase celerity and damping rate of the four models are analyzed and compared with the analytical solutions. The results show that the fourth-order dispersive Boussinesq-type equations have accurate linear phase celerity and damping rate. In particular, the model works in the range of $0 < kh < 6.19$ for damping rate and $0 < kh < 6.06$ for phase celerity.

Some preliminary numerical results are presented for the solitary wave propagating through a vertical porous breakwater. The calculated reflection and transmission coefficients are compared with published experimental data, the variation trend with wave height (H/h) is consistent with the measured values, and the agreements between the model result and experiment data are acceptable after selecting the appropriate coefficients.

Porous structures have an effect on the nonlinearity of waves propagation. The analysis of the nonlinear performance of the models and the implementation of the two-dimensional numerical model are left for further study.

References

1. Losada, I.J.; Patterson, M.D.; Losada, M.A. Harmonic generation past a submerged porous step. *Coast. Eng.* **1997**, *31*, 281–304. [CrossRef]
2. Gu, Z.; Wang, H. Gravity waves over porous bottoms. *Coast. Eng.* **1991**, *15*, 497–524. [CrossRef]
3. Lara, J.L.; Losada, I.J.; Liu, P.L.F. Breaking waves over a mild gravel slope: Experimental and numerical analysis. *J. Geophys. Res.* **2006**, *111*, C11019. [CrossRef]
4. Lynett, P.J.; Liu, P.L.F.; Losada, I.J. Solitary wave interaction with porous breakwaters. *J. Waterw. Port Coast. Ocean Eng.* **2000**, *126*, 314–322. [CrossRef]
5. Losada, I.J.; Lara, J.L.; Guanche, R.; Gonzalez-Ondina, J.M. Numerical analysis of wave overtopping of rubble mound breakwaters. *Coast. Eng.* **2008**, *55*, 47–62. [CrossRef]
6. Cheng, Y.Z.; Jiang, C.B.; Wang, Y.Y. A coupled numerical model of wave interaction with porous medium. *Ocean Eng.* **2009**, *36*, 952–959. [CrossRef]
7. Higuera, P.; Lara, J.L.; Losada, I.J. Three-dimensional interaction of waves and porous coastal structures using OpenFOAM®. Part I: Formulation and validation. *Coast. Eng.* **2014**, *83*, 243–258. [CrossRef]
8. Sasikumar, A.; Kamath, A.; Bihs, H. Modeling porous coastal structures using a level set method based VRANS-solver on staggered grids. *Coast. Eng. J.* **2020**, *62*, 198–216. [CrossRef]
9. Mohamed, K. A finite volume method for numerical simulation of shallow water models with porosity. *Comput. Fluids* **2014**, *104*, 9–19. [CrossRef]
10. Ren, B.; Wen, H.; Dong, P.; Wang, Y. Improved SPH simulation of wave motions and turbulent flows through porous media. *Coast. Eng.* **2016**, *107*, 14–27. [CrossRef]

11. Gao, J.L.; Zhou, X.J.; Zhou, L.; Zang, J.; Chen, H.Z. Numerical investigation on effects of fringing reefs on low-frequency oscillations within a harbor. *Ocean Eng.* **2019**, *172*, 86–95. [CrossRef]

12. Gao, J.L.; Ma, X.Z.; Zang, J.; Dong, G.H.; Ma, X.J.; Zhu, Y.Z.; Zhou, L. Numerical investigation of harbor oscillations induced by focused transient wave groups. *Coast. Eng.* **2020**, *158*, 103670. [CrossRef]

13. Gao, J.L.; Ma, X.Z.; Chen, H.Z.; Zang, J.; Dong, G.H. On hydrodynamic characteristics of transient harbor resonance excited by double solitary waves. *Ocean Eng.* **2021**, *219*, 108345. [CrossRef]

14. Buccino, M.; Tuozzo, S.; Ciccaglione, M.C.; Calabrese, M. Predicting Crenulate Bay Profiles from Wave Fronts: Numerical Experiments and Empirical Formulae. *Geosciences* **2021**, *11*, 208. [CrossRef]

15. Kirby, J.T. Boussinesq models and applications to nearshore wave propagation, surf zone processes and wave induced-current. In *Advances in Coastal Modelling*; Lakhan, V.C., Ed.; Elsevier Science: Amsterdam, The Netherlands, 2003; pp. 1–41.

16. Madsen, P.A.; Fuhrman, D.R. High-order Boussinesq-type modeling of nonlinear wave phenomena in deep and shallow water. In *Advances in Numerical Simulation of Nonlinear Water Waves*; Ma, Q.W., Ed.; World Scientific Publishing Co. Pte. Ltd.: Singapore, 2010; pp. 245–285.

17. Brocchini, M.A. reasoned overview on Boussinesq-type models: The interplay between physics, mathematics and numerics. *Proc. R. Soc. Lond. Ser. A Math. Phys. Eng. Sci.* **2013**, *469*, 20130496. [CrossRef]

18. Kirby, J.T. Boussinesq models and their application to coastal processes across a wide range of scales. *J. Waterw. Port Coast. Ocean Eng.* **2016**, *142*, 03116005. [CrossRef]

19. Sun, J.W.; Fang, K.Z.; Liu, Z.B.; Fan, H.X.; Sun, Z.C.; Wang, P. A review on the theory and application of Boussinesq-type equations for water waves. *Haiyang Xuebao* **2020**, *42*, 1–11. (In Chinese)

20. Gao, J.L.; Shi, H.B.; Zang, J.; Liu, Y.Y. Mechanism analysis on the mitigation of harbor resonance by periodic undulating topography. *Ocean Eng.* **2023**, *281*, 114923. [CrossRef]

21. Gao, J.L.; Ma, X.Z.; Dong, G.H.; Chen, H.Z.; Liu, Q.; Zang, J. Investigation on the effects of Bragg reflection on harbor oscillations. *Coast. Eng.* **2021**, *170*, 103977. [CrossRef]

22. Madsen, P.A.; Murray, R.; Sørensen, O.R. A new form of the Boussinesq equations with improved linear dispersion characteristics. *Coast. Eng.* **1991**, *15*, 371–388. [CrossRef]

23. Madsen, P.A.; Sørensen, O.R. A new form of the Boussinesq equations with improved linear dispersion characteristics. Part 2. A slowly-varying bathymetry. *Coast. Eng.* **1992**, *18*, 183–204. [CrossRef]

24. Nwogu, O. Alternative form of Boussinesq equations for nearshore wave propagation. *J. Waterw. Port Coast. Ocean Eng.* **1993**, *119*, 618–638. [CrossRef]

25. Schäffer, H.A.; Madsen, P.A. Further enhancements of Boussinesq-type equations. *Coast. Eng.* **1995**, *26*, 1–14. [CrossRef]

26. Zou, Z.L. Higher-order Boussinesq equations for rapidly varying topography. *Haiyang Xuebao* **2001**, *23*, 109–119. (In Chinese)

27. Liu, Z.B.; Sun, Z.C. Two sets of higher-order Boussinesq-type equations for water waves. *Ocean Eng.* **2005**, *32*, 1296–1310. [CrossRef]

28. Wei, G.; Kirby, J.T.; Grilli, S.T.; Subramanya, R. A fully nonlinear Boussinesq model for surface waves. Part I. Highly nonlinear unsteady waves. *J. Fluid Mech.* **1995**, *294*, 71–92. [CrossRef]

29. Gobbi, M.F.; Kirby, J.T.; Wei, G. A fully nonlinear Boussinesq model for surface waves. Part 2. Extension to O(kh)4. *J. Fluid Mech.* **2000**, *405*, 181–210. [CrossRef]

30. Lynett, P.J.; Liu, P.L.F. Linear analysis of the multi-layer model. *Coast. Eng.* **2004**, *51*, 439–454. [CrossRef]

31. Zou, Z.L.; Fang, K.Z. Alternative forms of the higher-order Boussinesq equations: Derivations and validations. *Coast. Eng.* **2008**, *55*, 506–521. [CrossRef]

32. Liu, Z.B.; Fang, K.Z. Two-layer Boussinesq models for coastal water waves. *Wave Motion* **2015**, *57*, 88–111. [CrossRef]

33. Madsen, P.A.; Bingham, H.B.; Liu, H. A new method for fully nonlinear waves from shallow water to deep water. *J. Fluid Mech.* **2002**, *462*, 1–30. [CrossRef]

34. Chazel, F.; Benoit, M.; Ern, A.; Piperno, S. A double-layer Boussinesq-type model for highly nonlinear and dispersive waves. *Proc. R. Soc. Lond. Ser. A Math. Phys. Eng. Sci.* **2009**, *465*, 2319–2346. [CrossRef]

35. Liu, Z.B.; Fang, K.Z. A new two-layer Boussinesq model for coastal waves from deep to shallow water: Derivation and analysis. *Wave Motion* **2016**, *67*, 1–14. [CrossRef]

36. Liu, Z.B.; Fang, K.Z.; Cheng, Y.Z. A new multi-layer irrotational Boussinesq-type model for highly nonlinear and dispersive surface waves over a mildly sloping seabed. *J. Fluid Mech.* **2018**, *842*, 323–853. [CrossRef]

37. Liu, Z.B.; Han, P.X.; Fang, K.Z.; Liu, Y. A high-order nonlinear Boussinesq-type model for internal waves over a mildly-sloping topography in a two-fluid system. *Ocean Eng.* **2023**, *285*, 115283. [CrossRef]

38. Cruz, E.C.; Isobe, M.; Watanabe, A. Boussinesq equations for wave transformation on porous beds. *Coast. Eng.* **1997**, *30*, 125–156. [CrossRef]

39. Hsiao, S.; Liu, P.L.F.; Chen, Y. Nonlinear water waves propagating over a permeable bed. *Philos. Trans. R. Soc. Lond. Ser. A* **2002**, *458*, 1291–1322. [CrossRef]

40. Chen, Q. Fully nonlinear Boussinesq-type equations for waves and currents over porous beds. *J. Eng. Mech.* **2006**, *132*, 220–230. [CrossRef]

41. Liu, Z.B.; Sun, Z.C. Wave propagating model over a porous seabed. *China Sci. Pap.* **2011**, *6*, 374–379. (In Chinese)

42. Klonaris, G.T.; Memos, C.D. Compound Boussinesq-type modelling over porous beds. *Appl. Ocean Res.* **2020**, *105*, 102422. [CrossRef]

43. Hsiao, S.; Hu, K.; Hwung, H. Extended Boussinesq Equations for Water-Wave Propagation in Porous Media. *J. Eng. Mech.* **2010**, *136*, 625–640. [CrossRef]

44. Fang, K.Z.; Huang, M.H.; Chen, G.L.; Wu, J.; Wu, H.; Jiang, T. Boussinesq Simulation of Coastal Wave Interaction with Bottom-Mounted Porous Structures. *J. Mar. Sci. Eng.* **2022**, *10*, 1367. [CrossRef]

45. Madsen, P.A.; Schäffer, H.A. Higher-order Boussinesq-type equations for surface gravity waves: Derivation and analysis. *Philos. Trans. R. Soc. Lond. Ser. A* **1998**, *356*, 3123–3184. [CrossRef]

46. Zou, Z.L.; Liu, Z.B.; Fang, K.Z. Further improvements to the higher-order Boussinesq equations: Bragg reflection. *Coast. Eng.* **2009**, *56*, 672–687. [CrossRef]

47. Peregrine, D.H. Long waves on a beach. *J. Fluid Mech.* **1967**, *27*, 815–827. [CrossRef]

48. Liu, Z.B.; Fang, K.Z.; Zou, Z.L. Boussinesq wave equations with full nonlinear characteristics at order O(μ2). *J. Harbin Eng. Univ.* **2012**, *33*, 556–561. (In Chinese)

49. Kirby, J.T.; Wei, G.; Chen, Q.; Kennedy, A.B.; Dalrymple, R.A. *FUNWAVE 1.0 Fully Nonlinear BOUSSINESQ Wave Model Documentation and User's Manual*; Report, Center for Applied Coastal Research; University of Delawar: Newwark, NJ, USA, 1998.

50. Vidal, C.; Losada, M.A.; Medina, R.; Rubio, J. Solitary wave transmission through porous breakwaters. In Proceedings of the 24th International Conference on Coastal Engineering, Costa del Sol-Malaga, Spain, 20–25 June 1988; pp. 1073–1083.

51. Lin, P.; Karunarathna, S.A. Numerical study of Solitary wave interaction with porous breakwater. *J. Waterw. Port Coast. Ocean Eng.* **2007**, *133*, 352–363. [CrossRef]